

Size-dependent polarization distribution in ferroelectric nanostructures: Phase field simulations

Jie Wang,^{1,a)} Marc Kamlah,¹ Tong-Yi Zhang,² Yulan Li,³ and Long-Qing Chen³

¹Forschungszentrum Karlsruhe, Institute for Materials Research II Postfach 3640, 76021 Karlsruhe, Germany

²Department of Mechanical Engineering, Hong Kong University of Science and Technology, Clear Water Bay, Kowloon, Hong Kong, People's Republic of China

³Department of Materials Science and Engineering, The Pennsylvania State University, University Park, Pennsylvania 16802, USA

(Received 13 February 2008; accepted 8 April 2008; published online 25 April 2008)

From phase field simulations, we investigate the size-dependent polarization distribution in ferroelectric nanostructures embedded in a nonferroelectric medium. The simulation results exhibit that vortex structures of polarizations and single-domain structures are formed in ferroelectric nanodots and nanowires, respectively. Furthermore, a single-vortex structure is formed in the ferroelectric nanodots if the aspect ratio of thickness to lateral size is less than a critical value, whereas the ferroelectric nanodots are in a multivortex state if the aspect ratio exceeds the critical value. When the aspect ratio approaches infinity, nanodots will become nanowires, in which polarizations are homogeneous. © 2008 American Institute of Physics. [DOI: 10.1063/1.2917715]

Nanoscale ferroelectric materials are receiving great interest from the academe and the industry due to their various potential applications to memory and storage devices, sensors, and actuators. The properties of low-dimensional ferroelectrics in nanometer scale substantially deviate from those of their bulk counterparts.¹⁻³ For example, ferroelectric nanodisks and nanorods exhibit vortex structures with the shrinking of the relevant lengths to the nanometer scale.³ The vortex structure in the nanoscale ferroelectrics, similar to the vortex structure in magnetic nanostructures, is regarded as a toroidal order which is different from the common homogeneous polarization order. The finding of the vortex in ferroelectric nanostructures opens exciting opportunities for designing nanomemory devices.⁴ The formation of the vortex structure depends on many factors, such as the sizes of the nanostructures and different boundary conditions.⁵ A solid understanding of size-dependent three-dimensional (3D) vortex structures in nanoferroelectrics is essential for their applications.

The properties of nanoscale ferroelectric materials are investigated through different theoretical approaches. For instance, first-principles and first-principles-derived methods are employed to study the properties of ferroelectric nanostructures.⁶⁻⁹ In addition to first-principles calculations, phenomenological approaches are effectively used to study ferroelectric materials at the nanoscale.¹⁰⁻¹² Phenomenological approaches can simulate ferroelectrics with larger size and are able to deal with problems with more complicated electrical and mechanical boundary conditions.¹³

In this letter, we present 3D simulations on the equilibrium polarization distribution in ferroelectric nanodots and nanowires with different sizes, which are embedded in a nonferroelectric medium by using a phenomenological phase field model that incorporates the long-range elastic and electrostatic interactions. In ferroelectric phase field simulations,¹⁴⁻¹⁶ it is often assumed that the mechanical

equilibrium is instantaneously established for a given polarization distribution. Therefore, the spontaneous polarization $\mathbf{P}=(P_1, P_2, P_3)$ is taken as the order parameter. The temporal evolution of the polarization pattern is calculated from the following time-dependent Ginzburg–Landau equation

$$\frac{\partial P_i(\mathbf{r}, t)}{\partial t} = -L \frac{\delta F}{\delta P_i(\mathbf{r}, t)} \quad (i = 1, 2, 3), \quad (1)$$

where L is the kinetic coefficient, F is the total free energy of the system, $\delta F / \delta P_i(\mathbf{r}, t)$ represents the thermodynamic driving force for the spatial and temporal evolutions of the simulated system, and \mathbf{r} denotes the spatial vector $\mathbf{r}=(x_1, x_2, x_3)$. The total free energy can be expressed as

$$F = \int_V [f_{\text{Lan}}(P_i) + f_{\text{grad}}(\partial P_i / \partial x_j) + f_{\text{elas}}(P_i, \varepsilon_{ij}) + f_{\text{elec}}(E_i, P_i)] dV, \quad (2)$$

in which f_{Lan} is the Landau free energy density, which is given by^{17,18}

$$\begin{aligned} f_{\text{Lan}}(P_i) = & \alpha_1(P_1^2 + P_2^2 + P_3^2) + \alpha_{11}(P_1^4 + P_2^4 + P_3^4) \\ & + \alpha_{12}(P_1^2 P_2^2 + P_2^2 P_3^2 + P_1^2 P_3^2) + \alpha_{111}(P_1^6 + P_2^6 \\ & + P_3^6) + \alpha_{112}[(P_1^4(P_2^2 + P_3^2) + P_2^4(P_1^2 + P_3^2) \\ & + P_3^4(P_1^2 + P_2^2))] + \alpha_{123}P_1^2 P_2^2 P_3^2, \end{aligned} \quad (3)$$

where α_1 is the dielectric stiffness and $\alpha_{11}, \alpha_{12}, \alpha_{111}, \alpha_{112}, \alpha_{123}$ are higher order dielectric stiffnesses. In Eq. (2), $f_{\text{grad}} = \frac{1}{2} g_{ijkl} (\partial P_i / \partial x_j) (\partial P_k / \partial x_l)$ is the gradient energy density, where g_{ijkl} are the gradient energy coefficients.¹⁶⁻¹⁸ It gives the energy penalty for spatially inhomogeneous polarization. $f_{\text{elas}} = \frac{1}{2} c_{ijkl} (\varepsilon_{ij} - \varepsilon_{ij}^0) (\varepsilon_{kl} - \varepsilon_{kl}^0)$ denotes the elastic energy density, where c_{ijkl} are the elastic constants, ε_{ij} are the total strains, and ε_{ij}^0 are the spontaneous strains or stress-free strains. The spontaneous strains are related to the spontaneous polarization components in the form of $\varepsilon_{ij}^0 = Q_{ijkl} P_k P_l$, where Q_{ijkl} are the electrostrictive coefficients.

^{a)} Author to whom correspondence should be addressed. Tel.: +49 7247 82 5857. FAX: +49 7247 82 2347. Electronic mail: jie.wang@imf.fzk.de.

cients. The crystal symmetry requires that all the odd-rank tensor coefficients are zero in the Landau–Devonshire free energy. Therefore, the first-rank tensor that represents piezoelectricity vanishes in the expression of spontaneous strains. The internal stresses generated by the inhomogeneous spontaneous strains are $\sigma_{ij}=c_{ijkl}(\varepsilon_{kl}-\varepsilon_{kl}^0)$. The stresses must satisfy the mechanical equilibrium equation of $\sum_{j=1}^3 \partial \sigma_{ij} / \partial x_j = 0$. The mechanical equilibrium equation is analytically solved by employing the general eigenstrain theory for a given polarization distribution under the periodic boundary condition.¹⁸ The last term in Eq. (2) is the self-electrostatic energy density, which is expressed as $f_{\text{elec}} = -\frac{1}{2} E_i P_i$,¹⁹ where E_i are three components of the electric field vector along the x_1 , x_2 , and x_3 directions, respectively. The self-electrostatic field is the negative gradient of the electrostatic potential, i.e., $E_i = -\partial \phi / \partial x_i$. The electrostatic potential is obtained by solving the following electrostatic equilibrium equation $\varepsilon_0(\kappa_{11} \partial^2 \phi / \partial x_1^2 + \kappa_{22} \partial^2 \phi / \partial x_2^2 + \kappa_{33} \partial^2 \phi / \partial x_3^2) = \partial P_1 / \partial x_1 + \partial P_2 / \partial x_2 + \partial P_3 / \partial x_3$, where ε_0 is the dielectric constant of vacuum and κ_{ii} denotes the relative dielectric constants of the material. In the electrostatic equilibrium equation, by assuming $\kappa_{ij}=0$ when $i \neq j$, the relative dielectric constant matrix is diagonal.¹⁹ The charge compensation is not considered in the present study because the ferroelectric nanostructures are assumed to be embedded in an electrically insulating medium, which means that all the simulations are conducted under the open-circuit boundary condition.

In the simulations, we employ $32 \times 32 \times N$ discrete grid points at a scale of $\Delta x_1 = \Delta x_2 = \Delta x_3 = 0.5$ nm to model the nanodots. The dot thicknesses are represented by the letter N in the x_3 direction. The nonferroelectric medium surrounding the ferroelectric nanodots is modeled to be 32 discrete grid points in the x_1 , x_2 , and x_3 directions with the grid size of 0.5 nm. Periodic boundary conditions in the x_1 , x_2 , and x_3 directions are employed for the outer boundaries of the nonferroelectric medium. For the ferroelectric nanowire, the discrete grid points and boundary conditions in the x_1 and x_2 directions are the same as those of the dots but a periodic boundary condition is directly applied to the ferroelectric wire in the x_3 direction without nonferroelectric medium in order to mimic the infinite length of the wire. The wire is discretized to 96 grid points in the longitudinal direction with the grid size of 0.5 nm. The material constants adopted in the present simulations are the same as those used in Ref. 19. The elastic and dielectric constants of the nonferroelectric medium are assumed to be the same as those of the ferroelectric nanostructures so that the solutions to the mechanical and electrostatic equilibrium equations can be analytically obtained.^{18,20} The interfaces between the ferroelectric nanostructures and the nonferroelectric medium are assumed as coherent. The zero boundary condition, i.e., $\mathbf{P}=0$, is used for spontaneous polarizations at the interfaces between the ferroelectric nanostructures and the nonferroelectric medium. The semi-implicit Fourier-spectral method²⁰ is employed to solve Eq. (1). In this letter, we present simulation results only at steady state and at room temperature.

Figure 1(a) shows the 3D polarization distribution in a 16×16 nm² square nanodot with a thickness of 8 nm along the x_3 direction, where every other polarization vector is plotted for clarity. The polarizations form a single-vortex pattern with the vortical axis perpendicular to the x_1x_2 plane. It is found that polarizations at the dot center and four corners have smaller magnitudes than those at other parts. It

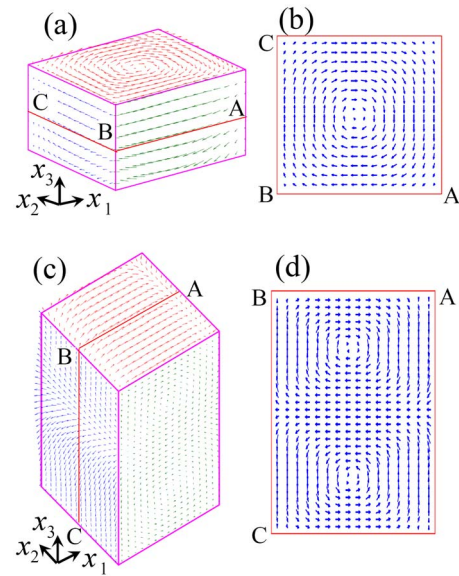


FIG. 1. (Color online) Polarization distributions of 16×16 nm² square nanodots with the thicknesses of [(a) and (b)] 8 nm and [(c) and (d)] 32 nm, respectively, in the x_3 direction. (a) and (c) are the 3D vortex structures; (b) and (d) are the 2D projections of polarizations in the middle planes of the corresponding dots.

should be noted that some polarizations in the x_1x_3 plane are not parallel to the x_1 axis. This result is different from that of the first-principles-derived effective Hamiltonian simulation, in which all polarizations are parallel to the x_1 axis for the freestanding dots with complete stress relaxation.²¹ The difference may be due to the present simulated dots assumed to be embedded in a nonferroelectric medium, while the dots are traction-free at surfaces in the first-principles-derived effective Hamiltonian simulations. Figure 1(b) gives the two-dimensional (2D) projection of polarizations in the middle plane perpendicular to the thickness direction. One can find that the polarizations form four domains with each side of the square. The four domains are separated by four 90° domain walls along the diagonals of the square. The maximal magnitude of the polarizations is located at the center of each domain. The average values of polarization components P_1 and P_2 in the dot are found to be approximately zero, while the toroidal moment of polarization in the x_3 direction is nonzero, which can be used as an order parameter in potential nanomemory devices.²²

In order to study the size-dependent polarization distribution, ferroelectric dots with different thicknesses are examined. Single-vortex structures that are similar to Fig. 1(a) are found for all dots with thickness of less than 16 nm ($N=32$). In the thickness range from 16 to 24 nm, the dots still have a single-vortex structure but the vortical axis changes its direction and becomes perpendicular to the x_1x_3 plane, which is not shown here due to page limitation. Figure 2 shows the number of vortices versus nanodot thickness. There is a change from a single-vortex state to a double-vortex state when the thickness increases from 24 to 30 nm, as shown in Fig. 2. Then, the double-vortex state remains in a range from 30 to 56 nm. With the thickness further increasing to 60 nm, three vortices are found in the ferroelectric nanodots. Figures 1(c) and 1(d) show a typical double-vortex structure of the 32-nm-thick dot and the corresponding 2D projection of polarizations in the middle plane parallel to the thickness direction. The axes of the two

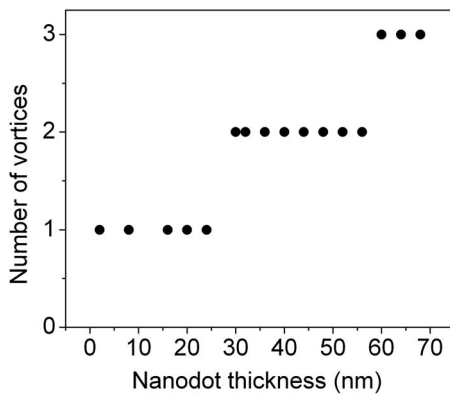


FIG. 2. Number of vortices vs nanodot thickness.

vortices are parallel to each other and both are perpendicular to the x_1x_3 plane. This result is different from that of the nanodot in Fig. 1(a), in which the polarizations form a single-vortex structure and the vortex axis is perpendicular to the x_1x_2 plane. Figure 1(d) shows that seven domains exist in the double-vortex structure with two vortices sharing one domain in the middle. The polarizations in the upper and lower vortices change their orientations clockwise and counterclockwise, respectively. This result is reasonable from the energy point of view. If both vortices had the same vortical direction, clockwise or counterclockwise, there must be an additional domain wall between them that would increase the total free energy of the system.

Figures 3(a) and 3(b) show the polarization distribution of a $16 \times 16 \text{ nm}^2$ square nanowire and the corresponding 2D projection of polarizations in the middle plane parallel to the wire length direction, respectively. The polarizations are found to be homogeneous along the wire. This is because the wire is infinitely long in the x_3 direction, thus, there is no depolarization field generated in this direction. When all polarizations are parallel to the wire, there are also no depolarization fields in the x_1 and x_2 directions. In this case, the energy of the nanowire is minimal in the homogenous state. The same result is also obtained by the first-principles-derived effective Hamiltonian simulation.⁵ Although all the polarizations are parallel to the longitudinal direction of the

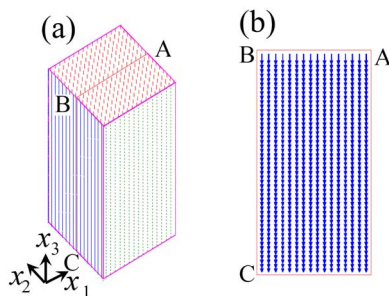


FIG. 3. (Color online) Polarization distribution of a $16 \times 16 \text{ nm}^2$ square nanowire. (a) 3D polarization distribution and (b) 2D projection of polarizations in the middle plane of the wire. The periodic boundary condition is used in the x_3 direction for the simulated ferroelectric nanowire.

wire, the polarization can be induced in the transversal direction by an external electric field, which will be stable for a period of time when the electric field is removed, if the surface charges are compensated by surrounding charges.²³

In summary, we demonstrate that the dipole vortex structures in ferroelectric nanodots are highly dependent on the dot size. For the ferroelectric nanodots with the size of 16 nm in both x_1 and x_2 directions, a single-vortex structure will be formed when the dot thickness is less than 24 nm in the x_3 direction. When the thickness increases from 24 to 30 nm, the ferroelectric nanodots change from a single-vortex state to a multivortex state. However, there is no vortex structure in a ferroelectric nanowire, in which polarizations are found to be homogeneous along the wire. The simulation results provide guidelines on how to obtain desirable vortex structures of polarizations by manipulating geometrical configurations, which might be crucial for the applications of nanoscale ferroelectric materials.

J.W. gratefully acknowledges the Alexander von Humboldt Foundation for awarding a research fellowship to support his stay at Forschungszentrum Karlsruhe. T.Y.Z. is grateful for the support from the Hong Kong Research Grants Council under the Grant No. G_HK015/06-II. L.Q.C. thanks the supports from the U.S. Department of Energy under the Grant No. DOE DE-FG02-07ER46417 and the National Science Foundation under the Grant No. DMR-0507146 and DMR 0708759.

¹W. L. Zhong, Y. G. Wang, P. L. Zhang, and B. D. Qu, *Phys. Rev. B* **50**, 698 (1994).

²I. Ponomareva, L. Bellaiche, and R. Resta, *Phys. Rev. Lett.* **99**, 227601 (2007).

³I. I. Naumov, L. Bellaiche, and H. Fu, *Nature (London)* **432**, 737 (2004).

⁴P. Ghosez and K. M. Rabe, *Appl. Phys. Lett.* **76**, 2767 (2000).

⁵I. Ponomareva, I. I. Naumov, and L. Bellaiche, *Phys. Rev. B* **72**, 214118 (2005).

⁶J. Junquera and P. Ghosez, *Nature (London)* **422**, 506 (2003).

⁷B. Meyer and D. Vanderbilt, *Phys. Rev. B* **63**, 205426 (2001).

⁸S. Prosandeev, I. Ponomareva, I. Korrev, I. Naumov, and L. Bellaiche, *Phys. Rev. Lett.* **96**, 237601 (2006).

⁹R. E. Cohen, *Nature (London)* **358**, 136 (1992).

¹⁰C. H. Ahn, K. M. Rabe, and J. M. Triscone, *Science* **303**, 488 (2004).

¹¹Y. G. Wang, W. L. Zhong, and P. L. Zhang, *Phys. Rev. B* **51**, 5311 (1995).

¹²S. Li, J. A. Eastman, Z. Li, C. M. Foster, R. E. Newnham, and L. E. Cross, *Phys. Lett. A* **212**, 341 (1996).

¹³J. Wang and T. Y. Zhang, *Appl. Phys. Lett.* **88**, 182904 (2006).

¹⁴R. Ahluwalia and W. Cao, *J. Appl. Phys.* **93**, 537 (2003).

¹⁵Y. L. Li, S. Y. Hu, Z. K. Liu, and L. Q. Chen, *Appl. Phys. Lett.* **78**, 3878 (2001).

¹⁶S. Nambu and D. A. Sagala, *Phys. Rev. B* **50**, 5838 (1994).

¹⁷J. Wang and T. Y. Zhang, *Phys. Rev. B* **73**, 144107 (2006).

¹⁸J. Wang, S. Q. Shi, L. Q. Chen, Y. L. Li, and T. Y. Zhang, *Acta Mater.* **52**, 749 (2004).

¹⁹Y. L. Li, S. Y. Hu, Z. K. Liu, and L. Q. Chen, *Appl. Phys. Lett.* **81**, 427 (2002).

²⁰H. L. Hu and L. Q. Chen, *J. Am. Ceram. Soc.* **81**, 492 (1998).

²¹S. Prosandeev and L. Bellaiche, *Phys. Rev. B* **75**, 094102 (2007).

²²J. F. Scott, *Nat. Mater.* **4**, 13 (2005).

²³J. E. Spanier, A. M. Kolpak, J. J. Urban, L. Grinberg, L. Ouyang, W. S. Yun, A. M. Rappe, and H. Park, *Nano Lett.* **6**, 735 (2006).